Organic Photoconductor Evaluation Technology: Latent Image Evaluation

Koichi Aizawa † **Tomoki Hasegawa** †

ABSTRACT

It is important that printing be made possible at high resolution to make electrophotographic machines faster, color image compatible, and expand the printing field,. Fuji Electric has developed a MASPP (Micro Area Surface Potential Probe) and an EFM (Electrostatic Force Microscope) to understand the mechanism of electrical latent image formation more clearly. The photoconductor surface charge is changed by the irradiation of laser light. MASPP detects the change of the charge as a current induced by it In the case of a high mobility photoconductor, the latent image potential was shown to be spread-out spatially to a greater extent than the potential distribution that corresponds to the exposure. In the case of a low mobility photoconductor, the distribution of surface potential was found to be more precise and similar to the surface potential distribution that closely corresponds to the exposure.

1. Introduction

Electrophotographic devices are increasingly becoming faster and supporting color. It is vital to increase the resolution of electrophotographic devices in order to support photo-quality images in the light-printing field, where growth is expected. The latent-image formation mechanism on photoconductors greatly affects print resolution, and elucidation of this mechanism is vital for improving resolution. Fuji Electric has reported the results of evaluating latent-image formation using a micro area surface potential probe (MASPP)[(1)~(3)], which applies the principle of measuring the changes in the photoconductive surface potential upon illumination with a detection laser as induced current[(4)].

Fuji Electric have improved the exposure system of the MASPP method, and performed measurements with the latent-image formation changed arbitrarily, and triangle-wave exposure applied. Differences between the applied voltage and surface potential on the photoconductor were measured via the surface-potential measurement method using an electrostatic force microscope (EFM), in order to confirm the phenomenon whereby larger the charge mobility causes a larger horizontal spread of surface potential[(1),(2)]. As a result, they confirmed that the surface potential spreads wider than applied voltage in high-mobility photoconductor, and the surface potential is faithful to the applied voltage in low-mobility photoconductors.

This is an important result, showing that it is not possible to rely on higher mobility alone as the direction for designing photoconductors for high-speed machines.

Fig.1 MASPP Principle

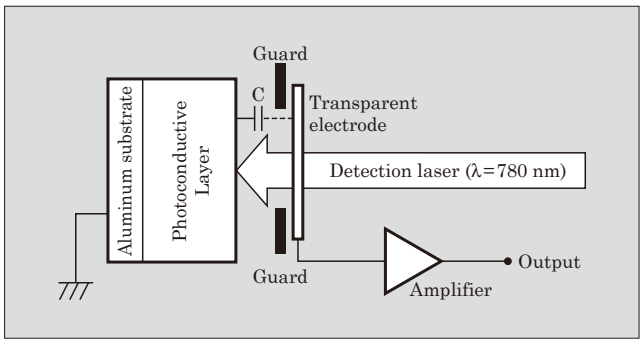

2. The Micro Area Surface Potential Probe (MASPP) Method

2.1 Measuring Equipment and Methods

This section describes the equipment for measuring latent images using the MASPP method.

Fig.2 Relationship between Surface Potential and Induced Current

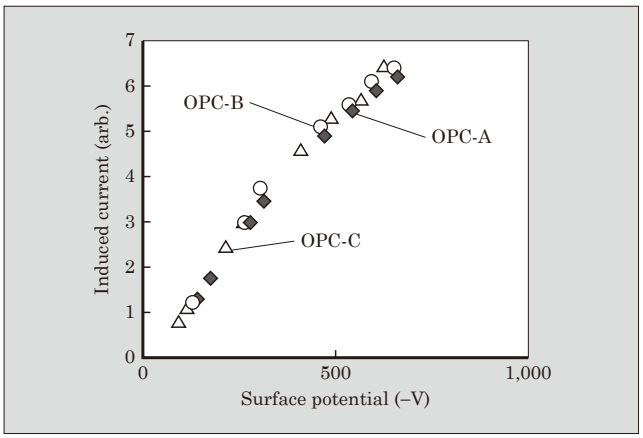

† MONOTSUKURI Strategy Division Fuji Electric Holdings Co., Ltd.

Figure 1 shows the structure of the probe for measuring the micro area surface potential. A transparent electrode is installed opposite to a charged photoconductive surface forming a capacitor. The surface potential decays, and changes occur, as a result of light exposure (laser with 10 μm diameter and wavelength of 780 nm) passing through the transparent electrode. At this time, the induced current is measured through an amplifier.

Figure 2 shows the relationship between the photoconductive surface potential and the induced current. The surface potential can be detected by measuring the induced current.

For the current research, the source of latent-image exposure light to the photoconductive surface was changed from the laser scanning unit (LSU) of a conventional commercially available laser printer to a line beam with width of 10 μm and length of 4,000 μm. It was possible to create an arbitrary exposure shape by controlling the light power of this beam.

The latent-image potential of a dual-layer negative-charge organic photoconductor when exposed to a triangle waveform was measured, and the changes in the depth and width of the latent image in response to changes to the organic photoconductor's charge transport material (CTM) and the amount of exposure light were investigated.

As shown in Fig. 3, exposure to the triangle waveform was performed, reducing the laser light power linearly from 100% to 0%. At a light power of 100%, the exposure was changed to 100, 133, 166, and 200 μW.

Fig.3 Triangle Waveform Exposure Profile

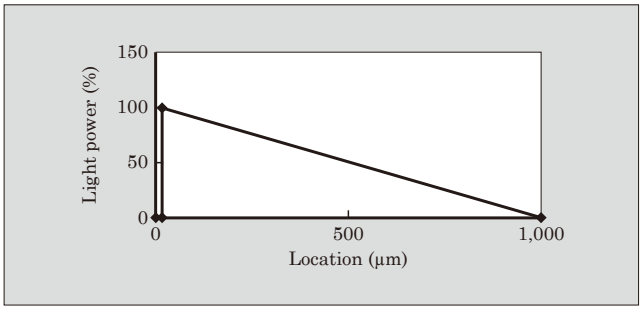

Table 1 Mobility and Photoconductor Properties of Each Sample

CTM	Sample No.	Mobility [10^{-6}cm^2/(V–s)]	E_{300} (mJ/m^2)	E_{100} (mJ/m^2)	V_{r5} (–V)
Low mobility	L-1	1.1	1.70	7.70	31
	L-2	5.4	1.40	2.70	13
	L-3	21.4	1.10	2.20	11
High mobility	H-1	3.1	1.20	3.20	16
	H-2	73.3	1.20	2.50	14
	H-3	106.9	1.20	2.10	10

*E_{300}: Light power required for decay of –600 V to –300 V
E_{100}: Light power required for decay of –600 V to –100 V
V_{r5}: Residual potential after exposure of 50 mJ/m^2

2.2 Measurement Photoconductor

A sample was fabricated, with a structure consisting of a 30 mm diameter aluminum pipe, and the following charge generation layer (CGL) and charge transfer layer (CTL).

CGL: Thytanil phtalocyanine
Poly-vinyl-Buthyral
CTL: Charge transport material (CTM)
Bisphenol Z type Polycarbonate

Two types of charge transport material were used (high mobility and low mobility), in order to investigate the relationship between the CTL's charge mobility and the latent image. Samples with differing charge mobility were further created by changing the mixing ratio of the charge transport material and polycarbonates.

Table 1 shows the mobility and photoconductor properties of each sample. The property definitions are as follows.

E_{300}: Light power required for decay of –600 V to –300 V
E_{100}: Light power required for decay of –600 V to –100 V
V_{r5}: Residual potential after exposure of 50 mJ/m^2

Fig.4 Light Exposure Dependence

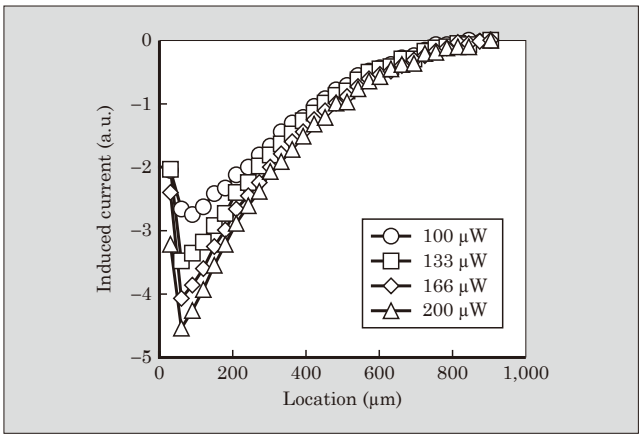

Fig.5 Definitions of Width and Depth in Latent Images

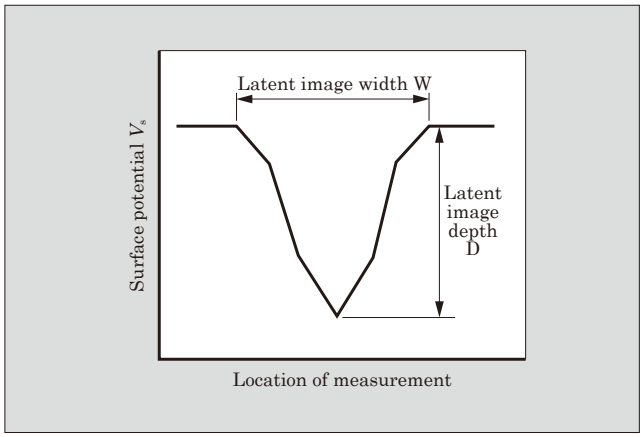

2.3 MASPP Measurement Results and Observations

(1) Light exposure dependence

Figure 4 shows the light-exposure dependence of sample H-3's latent-image potential (∝ induced current). The horizontal axis is the measured location, and the vertical axis is the induced current. A latent image was formed corresponding to the triangle wave. The figure shows that when the light exposure is increased from 100 μW to 200 μW, the induced current increases, and the latent image becomes deeper. At the same time, the width of the latent image also increases in accordance with the light exposure.

The depth and width of the latent image discussed here are as defined in Fig. 5. This is able to explain the decay in surface potential consequent to the increase in light exposure and the increase in density and thickness of the dots or lines in the actual printed image.

Figure 6 shows the latent-image potential (∝ induced current) when the mixing ratio of CTM and resin are changed in the CTL using a low-mobility CTM. At this time, the latent-image formation exposure is 200 μW. The increase in mobility from L-1 to L-3 makes the latent image deeper and wider.

(2) Mobility dependence of latent-image shape

Figs. 7 and 8 show the correlation between the latent-image width and depth of each sample, and the mobility.

Although the width of the latent image increases with the increase in mobility, there is little change in the depth of the latent image. Although the generated carrier in the photoconductive layer may be a large factor in the depth of the latent image, in this experiment, the CGL was kept constant, so it is possible that no difference was noted.

(3) Mobility dependence of latent-image resolution

Next, it was hypothesized that resolution is indicated by the charge level per unit of area, in order to associate the actual printed resolution with the latent-image shape. In order to quantify the resolution, it was defined as follows.

Resolution = depth of latent image / width of latent image^2

This formula shows that the deeper the latent image, and the smaller its area (proportional to the square of the width), the sharper the latent-image will be rendered. Figure 9 shows the mobility dependence of resolution.

It was shown that as the mobility increases, the resolution decreases.

Fig.6 Changes in Latent Image when Mobility is Changed

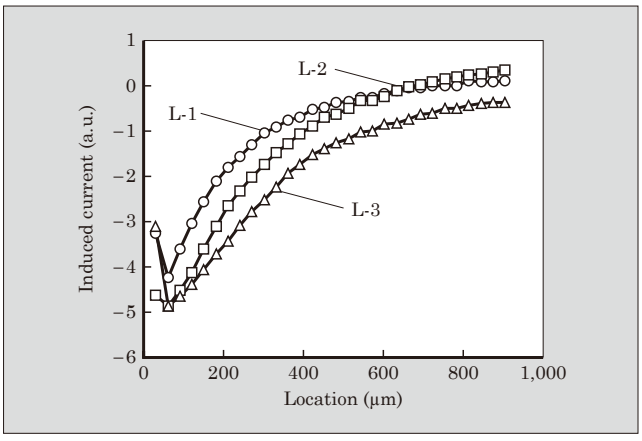

Fig.8 Dependence of Latent Image Width on Mobility

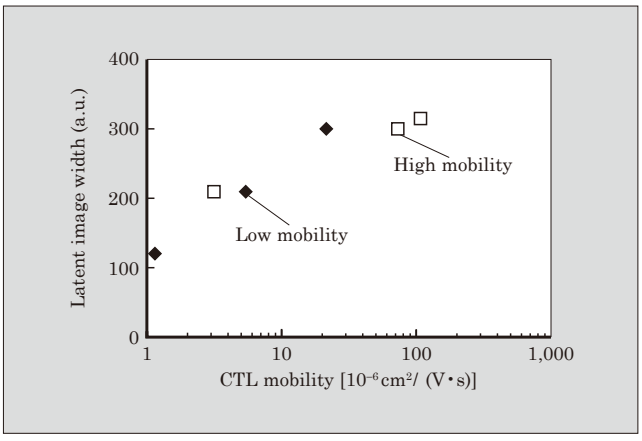

Fig.7 Dependence of Latent Image Depth on Mobility

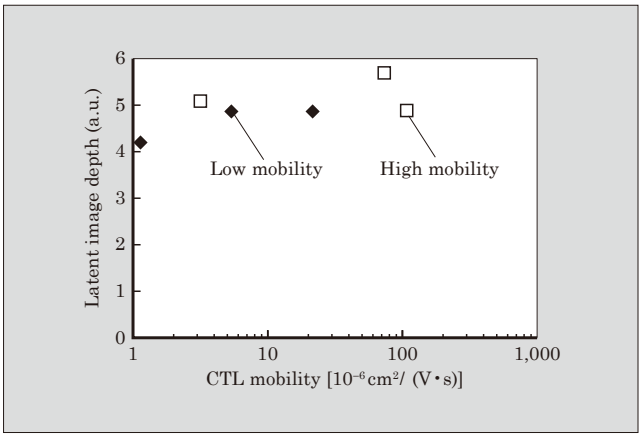

Fig.9 Dependence of Resolution on Mobility

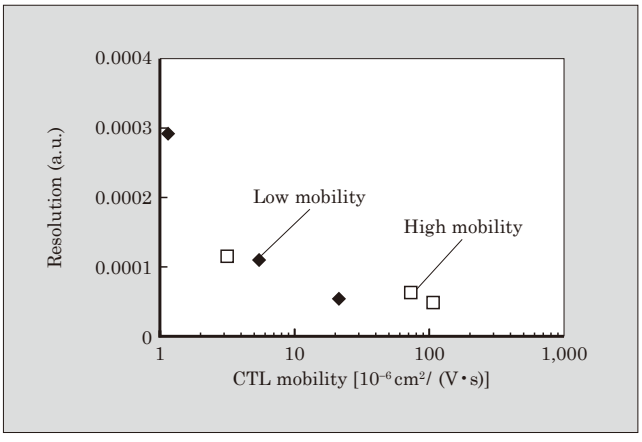

3. Electrostatic Force Microscope (EFM) Method

3.1 Principle of EFM Measurement

Figure 10 illustrates the principle of electrostatic force microscopy[5]~[7]. Under this method, when a cantilever to which is applied DC bias V_{DC} and AC bias V_{AC} sin ωt approaches a charged sample, the electrostatic induction of the tip generates electrostatic force, which bends the cantilever. The amount of bending is then detected via the optical lever method.

The applied AC bias frequency component $F\omega$ and twice higher frequency component F2ω that act on the cantilever are expressed by the following formula, using the parallel plane model in Fig. 11.

$$F_\omega = \frac{V_{DC} - pd_0/\varepsilon_0}{\{d-(1-\varepsilon_0/\varepsilon)d_0\}^2}\varepsilon_0 S V_{AC}\sin\omega t \quad \cdots\cdots (1)$$

$$F_{2\omega} = \frac{1}{4\{d-(1-\varepsilon_0/\varepsilon)d_0\}^2}\varepsilon_0 S V^2{}_{AC}\cos 2\omega t \quad \cdots\cdots (2)$$

$F\omega$: Applied AC bias frequency component acting on the cantilever
$F2\omega$: Twice higher frequency component acting on the cantilever
V_{DC} : DC bias, tip potential
V_{AC} sinωt : AC bias
d : Distance between tip end and bottom electrode
d_0 : Sample thickness
d-d_0 : Distance between tip and sample
ε : Dielectric permittivity
ε_0 : Vacuum permittivity
ρ d_0/ε : Sample potential
S : Surface area of tip end

If the distance between the tip and sample (d-d_0) and dielectric permittivity ε are known, then it is possible to measure $F\omega$ keeping V_{DC} constant, and calculate sample potential $\rho d_0/\varepsilon$ via formula[1].

When measuring with the high voltage, there is a large difference in the potentials of the tip V_{DC} and the sample, and there is a risk of discharges. Here, it is possible to perform measurements without causing discharge, by a zero voltage method calculating the V_{DC} at which $F\omega=0$.

The cantilever was made by using the focused ion beam (FIB) method on 5 μm thick nickel foil.

3.2 Details of Sample for EFM Method

Here, in order to discuss the movement of charge in the charge transport layer, a sample was fabricated by coating an aluminum substrate with a charge transport layer (film thickness 5 μm) consisting of CTM and a binder resin (Z type polycarbonate) in a 1-to-1 mixture by mass. The charge mobility of the sample as calculated by the Time of Flight method is as follows.

a-1: 10^{-4} cm²/(V·s); High-mobility sample
d-1: 10^{-5} cm²/(V·s); Low-mobility sample

The electrodes were formed via vacuum deposition of aluminum on the charge transport layer. Details are shown in Fig. 12.

Electrodes A, B, and C are all connected to different power sources, and potential can be applied assuming a latent image.

The distance between the cantilever and sample surface was set at 5 μm, and the measurement was performed by moving horizontally at a 2 μm pitch.

3.3 Results of EFM Measurement and Observations[8]

(1) Changes in potential in the charged and non-charged areas

A voltage −150 V was applied to electrode A only (equivalent to general OPC voltage boundary of 30 V/μm), and no voltage was applied to electrodes B or C.

Fig.10 Principle of EFM Measurement

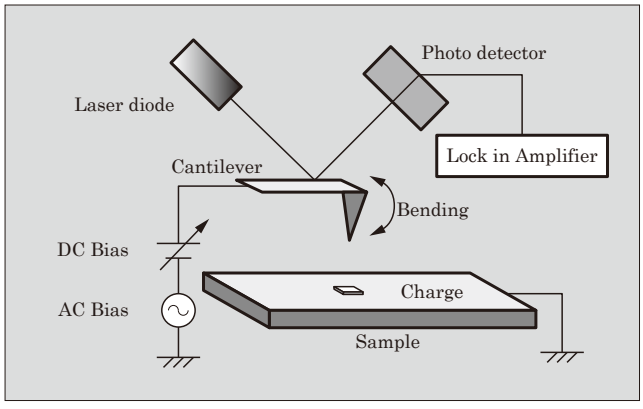

Fig.11 Parallel plane model

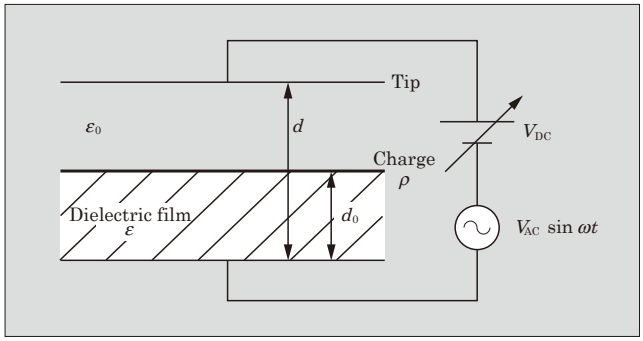

Fig.12 Structure of Samples for EFM Measurement

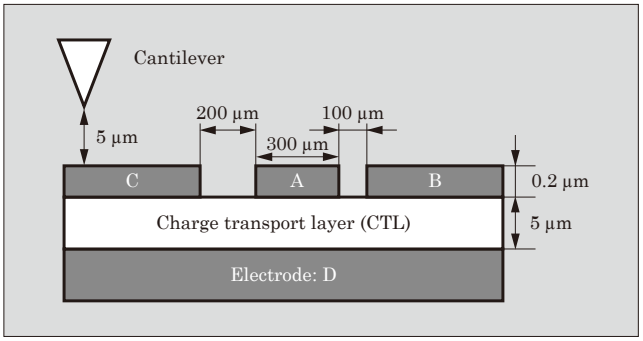

The results are shown in Figs. 13 and 14. The interval between the first and second times is 40 minutes. The low-mobility sample had potential close to the applied voltage, and there was also little difference between the first and second times (Fig. 13).

Meanwhile, for the high-mobility sample, the potential between electrodes A and B, and between electrodes A and C rose starting from the first time, as an effect from electrode A. On the second time, it spread even further in the horizontal direction (Fig. 14).

It is possible that this result suggests that high-mobility samples are susceptible to horizontal charge mobility.

(2) Changes in the charged area and intermediate part of the charged area

Figs. 15 and 16 show the results when −150 V were applied to electrodes A and B, and no voltage was applied to electrode C.

In the low-mobility sample, there is a −30 V valley between electrodes A and B on the first time, and the potential is near to the applied voltage. On the second time, the valley becomes shallower, at −70 V, indicating that the potential contrast may have favorable reproducibility.

This matches the results to date, with high-definition latent images in low-mobility photoconductors.

Meanwhile, with the high-mobility sample, electrodes A and B had the same potential between them on the first measurement, and no valley was noted in the potential. This matches past results in which there is a large horizontal spread in the latent image in high-mobility photoconductors.

These results suggested the possibility that charge is being transported from the charged electrode to the non-charged electrode. Thus voltage (−150 V) was applied to electrodes A and B, making them charged electrodes, and the dependence of the potential of the non-charged area between electrodes A and B on elapsed time was investigated. The results are shown in Fig. 17.

In the low-mobility sample, although the potential was found to gradually rise as voltage was applied to electrodes A and B, it did not reach the applied voltage (−150 V) even after 2,200 seconds.

In the high-mobility sample, a rapid rise in potential was observed, reaching the applied voltage after 136 seconds. It is possible that this was because the charge applied to electrodes A and B is easily transported horizontally on the surface or in the charge transport layer.

These results have shown a way ahead for materials development.

Fig.13 Surface Potential of Low Mobility Sample

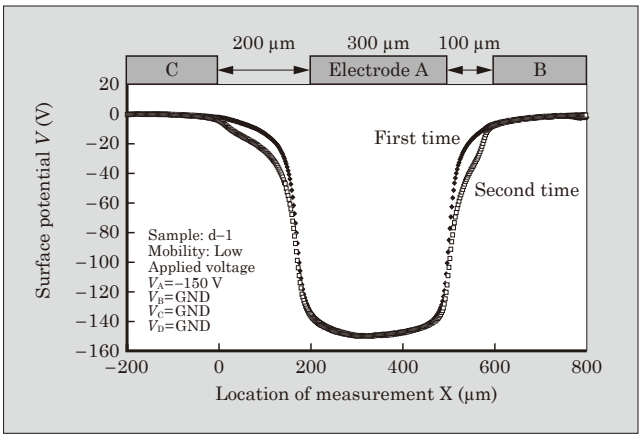

Fig.14 Surface Potential of High Mobility Sample

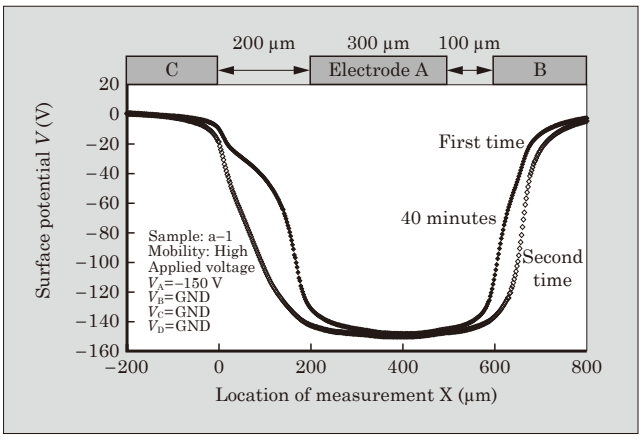

Fig.15 Surface Potential of Low Mobility Sample

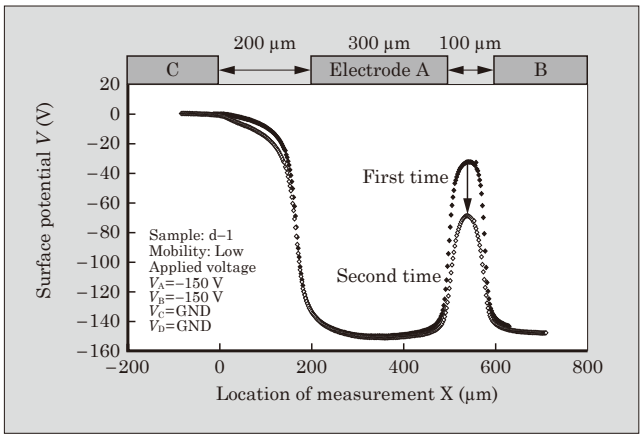

Fig.16 Surface Potential of High Mobility Sample

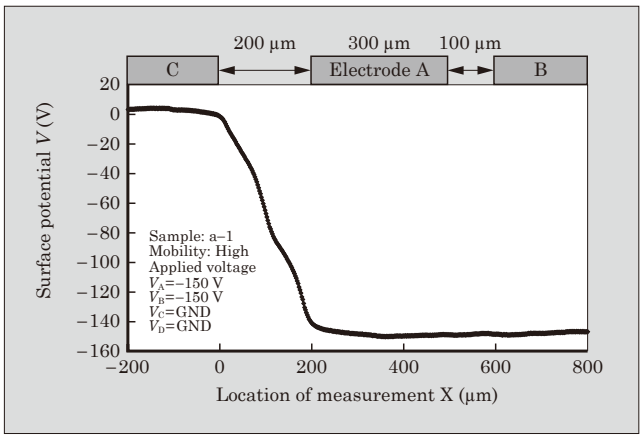

Fig.17 Changes over Time of Surface Potential at Intermediate Point between Electrodes A & B

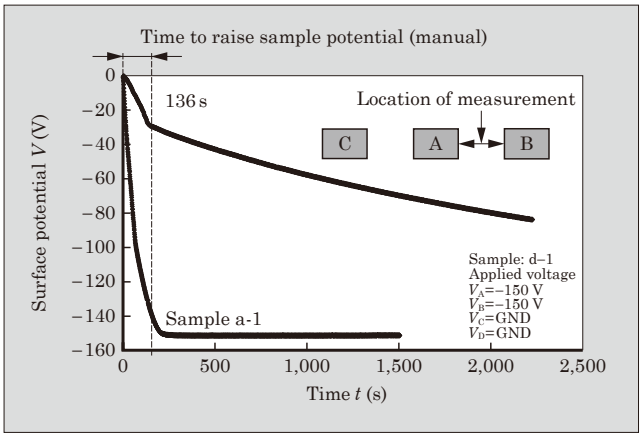

4. Conclusions

(a) Latent images corresponding to a triangle waveform exposure profile were obtained, enabling arbitrary exposure light shapes to be formed via a 10 μm-wide line beam using the MASPP method. The latent images were found to be dependent on the light exposure power and photoconductor properties.

(b) Increasing the photoconductor charge mobility was found to rapidly increase the latent-image width and slightly increase the latent-image depth, and caused the latent-image resolution to fall.

(c) Using the EFM method, it is possible to measure surface potential with a resolution of 2 μm.

(d) The status of the surface potential on the charge transport layer in response to applied voltage differed according to the charge mobility. With a low-mobility charge transport layer, the surface potential was near to the applied voltage, while with a high-mobility charge transport layer, it spread horizontally beyond the applied voltage.

(e) From these results, the authors conclude that charge has high horizontal mobility in high-mobility photoconductors, causing large widening of the latent image.

5. Postscript

Moving forward, Fuji Electric will work to quantify the charge transport path and level of charge transport, by collecting data on samples with differing mobility, and clarifying the charge-transport mechanism that contributes to changes in surface potential. Fuji Electric further intends to utilize this research to help offer photoconductors that achieve high resolution from the contrast with the latent-image formation mechanism.

References

(1) Takeshima, M. and Aizawa, K. Evaluation of 1-dot Latent Image Potential. The Imaging Society of Japan, Japan Hardcopy. 2001, pp.281-284.

(2) Aizawa, K. et al. A study of 1-dot latent image potential. Proceeding of NIP17 International Conference on Digital Printing Technologies. 2001, pp.572-575.

(3) Aizawa, K. et al. A Study of Latent Image Analysis Technologies. The Imaging Society of Japan. Imaging Conference Japan 2008 Fall Meeting. 2008, pp.33-36.

(4) Lin, C.W. and Nozaki, T. Proceedings of IS&T's 11th International Congress on Advances in Non-Impact Printing Technologies. 1995, p.138.

(5) Uehara, T. et al. A Study of Measurement of High Voltage Potential Distribution Using Electrostatic Force Microscopy. The Imaging Society of Japan, Japan Hardcopy. 2000, pp.72-75.

(6) Uehara, T. et al. Methods for Measuring Surface Potential in Electrostatic Force Microscopy. Annual Meeting of the Institute of Electrostatics Japan. 2003, pp.49-52.

(7) Uehara, T. et al. Methods for Measuring Surface Potential in Electrostatic Force Microscopy. The Imaging Society of Japan, Japan Hardcopy 2004 Fall Meeting. 2004, pp.41-44.

(8) Aizawa, K. et al. A Study of Latent Image Analysis Technologies Using Electrostatic Force Microscopy Method. The Imaging Society of Japan. Imaging Conference Japan 2009 Fall Meeting. pp.29-32.